Optical System for Detection and Classification of Surface Defects in Ferrites

L. Chmielewski[1], M. Skłodowski[1], W. Cudny[1], M. Nieniewski[1], A. Jóźwik[2]

Abstract Methods of visual detection and measurement of certain surface defects of ferrite products are presented. Difficulties such as dark colour of ferrite and variability of appearance of defects under different light conditions have been overcome. The monochromatic images of the product surface, taken under a highly specialised lighting system with a standard monochromatic digital camera, are processed with a hierarchical morphological irregularity detector, classified with a feature-based *k* nearest neighbours classifier, and postprocessed. The same methodology can be applied to other materials of similar (magnets) or different appearance.

1. Motivation

Ferrites are ceramic magnetic materials made of oxide powders. Ferrite cores are manufactured by compacting and sintering these powders, and by grinding some surfaces to required dimensions. The aim of the paper is a presentation of the methods of detection and measurement of certain surface irregularities which emerge in the manufacturing process [FMCL97]. The main difficulties encountered are: dark colour of ferrite, large variety of possible shapes and locations of defects, and variability of their appearance, even in typical light conditions.

The above circumstances have effectively prevented even the leading manufacturers of ferrites from automating the surface quality inspection of ferrite cores.

Manufacturers and buyers of ferrite cores distinguish tens of classes of defects (of various surfaces, of shape, of the material itself). Standardisation bodies work on defining these defects, but their work is still far from finished.

In this research, *only some mating surfaces defects* will be considered. The reason is twofold: 1^o this class of defects seemed tractable; 2^o the final user of the Project results, that is, POLFER Magnetic Materials Co.Ltd., Warsaw, has carried out an extensive query among the manufacturers to find out which defects are of greatest importance and interest. And the defects of *mating surfaces* (surfaces with which cores that form two halves of a magnetic circuit should touch) appeared to be the most frequently indicated. In this way, the possibility and the need have successfully met one another.

In setting the acceptable dimensions of defects two types of criteria are usually taken into account. These are: proper operation of the product, and its appearance. In many cases the latter is more demanding, as in some locations quite large defects do not impair the functionality of a core. The fact that some defects are acceptable gave rise to the use of a notion of *irregularity*, to avoid the negative connotation of the word *defect*.

Although the presented study concerns ferrites, the same methodology can be used to investigate defects on flat surfaces in other similar materials, such as magnets. Completely different surfaces: white ceramics, painted surfaces, would also be tractable.

[1] Institute of Fundamental Technological Research, PAS (http://www.ippt.gov.pl) and Association for Image Processing (http://www.tpo.org.pl).

[2] Institute of Biocybernetics and Biomedical Engineering, Polish Academy of Sciences (adamj@ibbrain.ibb.waw.pl).

2. Overview of the applied methods

The monochromatic images of the irregularities of interest are acquired by the system consisting of a highly specialised lighting set-up, a standard digital camera, and a computer.

A hierarchical method for classification of a core with respect to surface irregularities has been applied. It consists of two main phases:

- **Detection phase.** Regions which might be a defect are detected. This phase is hierarchical in itself: the morphological pyramid technique has been used [Nie97]. In detecting the defects of different sizes the structuring elements are kept the same, but the image is scaled down, to reduce the time of computations.
- **Classification phase.** Pixels of the regions selected in the detection phase are classified with a highly advanced version of the *k nearest neighbours* method [Joz83, Joz96]. The features used were selected from a large number of possible deterministic, statistical and textural measures, with the use of numerous training samples.

The whole method is complemented by **postproccessing** the results of the classification phase: nearby blobs are linked and convex hulls of the result is found.

Finally, the defects are measured, and the results are compared with quality standards to get the final classification of the product as belonging to a respective quality class. Quantitative nature of the measurements make them useful in analysis of the production process.

3. Types of defects

A pair of cores with their mating surfaces visible can be seen in Fig. 1. Two types of irregularities are of main importance on mating surfaces: *chips* and *pull-outs*.

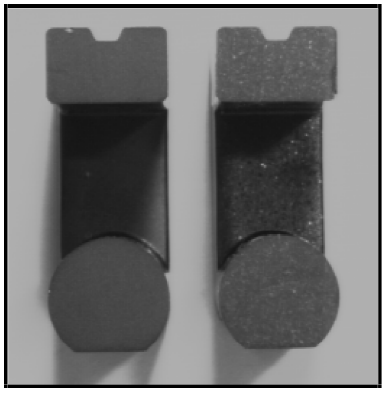

Fig. 1. Cores with their mating surfaces visible

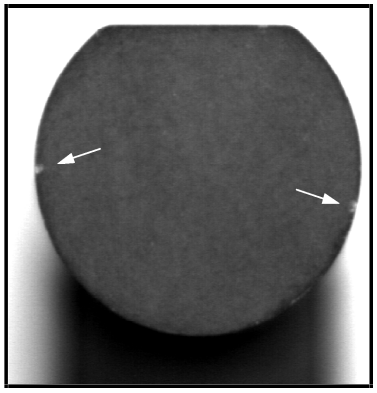

Fig. 2. Example of chips

A *chip* emerges where the material has been removed in the way of brittle cracking during grinding or as a result of another mechanical impact.

A *pull-out* is a place from which the material has been taken away by a stamp during the pressing process (the soft material has stuck to the stamp).

As far as the mating surfaces are considered, the two types of defect can be indiscernible. Although they arise in different places of the production line, one can accompany another: a chip can appear where the material has been previously weakened by a partial pull-out in form of an undersurface defect. This is exemplified by Fig. 4. Moreover, the influence of the two types of defects on the quality of the final product is the same. Consequently, in this case the chips and the pull-outs can be treated together.

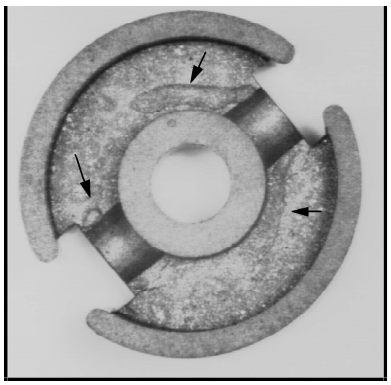

Fig. 3. Pull-outs on inner surface

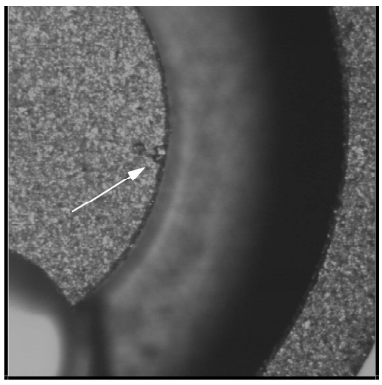

Fig. 4. Chip or pull-out? (see text)

4. The problem of lighting

Because of the dark colour of the investigated objects, the proper lighting becomes vital. In designing the lighting system the following criteria have been taken into account:

1. maximum insensitivity to position and direction of the object in the field of view;
2. insensitivity to change of distance between the tested surface and the camera (within some range);
3. possibly large contrast of defects;
4. possibly large difference between irradiation of the tested surface and of other visible surfaces on the tested object and the base.

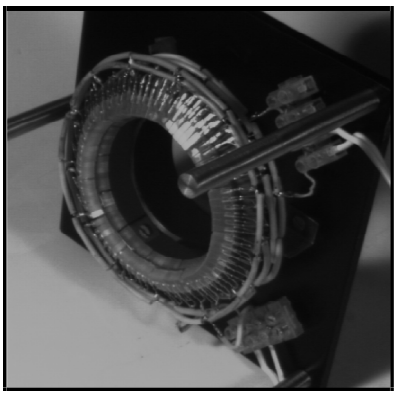

Fig. 5. Double Layered LED Illuminator (DLEDI) bottom view

Fig. 6. Variable Light Beam Illuminator (VLBI) side view

Due to the above criteria (mainly 3 and 4), after some experiments a lighting similar to natural diffused light has been excluded. Six circular lighting systems have been designed and manufactured or bought [Eps97]. The two tangential light systems have been selected as the best ones: the Double Layered LED Illuminator (DLEDI), Fig. 5, and the Variable Light Beam Illuminator (VLBI), Fig. 6. Both illuminators provide for a very uniform irradiation of the tested surfaces (see Fig. 7), while the VLBI better meets the requirements 3 and 4. The results presented in this present paper have been obtained with the VLBI.

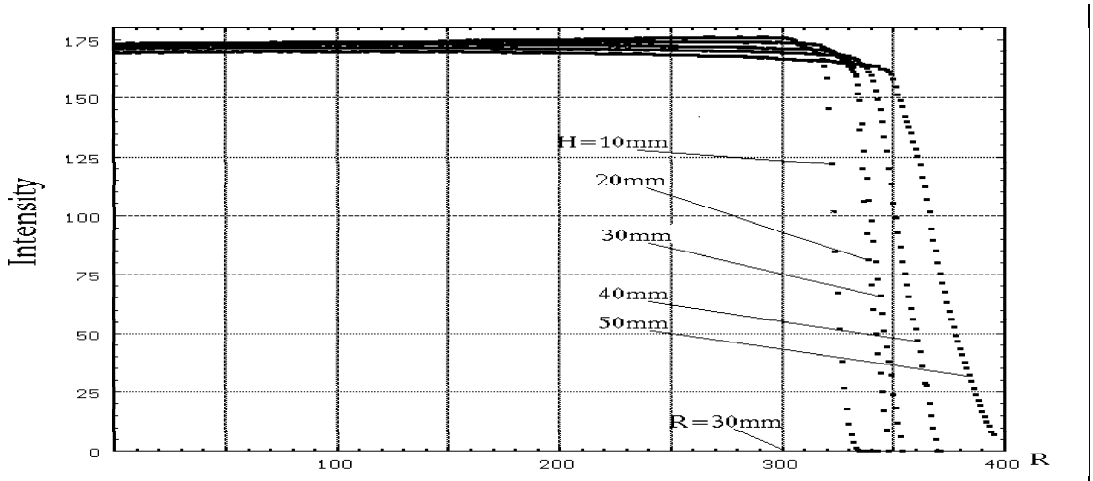

Fig. 7. A very good uniform radial illumination distribution for the DLEDI at various distances H from camera to object surface, at f = 25 mm, A = 1.8. Similarly for VLBI

5. The morphological defect detector

The defect detection system for inspection of ferrite cores includes three major components:

1. morphological defect detector;
2. morphological pyramid;
3. software for data reduction.

A comprehensive description of these components is given in [Nie97]. In the following, only a general description of the defect detection system is presented.

The principle of operation of the morphological defect detector is based on the following equation

$$T = I - \min[(I \bullet S) \circ S, I] \tag{1}$$

where I denotes the input image of the ferrite core, S is the structuring element, and T is the output image, called a gray level map of defects. In the above equation $(A \bullet I)$ denotes the closing of the image A by the structuring element I, and $(A \circ I)$ denotes the opening of the image A by the structuring element I. Eq. (1) allows one to detect defects brighter than the surroundings. An analogous equation can be used for detecting defects darker than the surroundings. The map of defects T indicates both the position of the defective pixels as well as the strength of a defect (also called the measure of defectiveness) at a given pixel. This measure is equal to zero in a defect-free area and is greater than zero if a defect is detected. The limitations of the presented defect detector stem from the fact that the detector gives a noisy output – indicating numerous and relatively mild defects in the areas where the human does not see any defect. Furthermore, using the structuring element of finite dimensions, one is able to detect defects slightly greater than the structuring element, which typically has the form of a flat 3*3 square. Detection of significantly larger defects would require a larger structuring element, which would result in a sharp increase of the processing time for a given image.

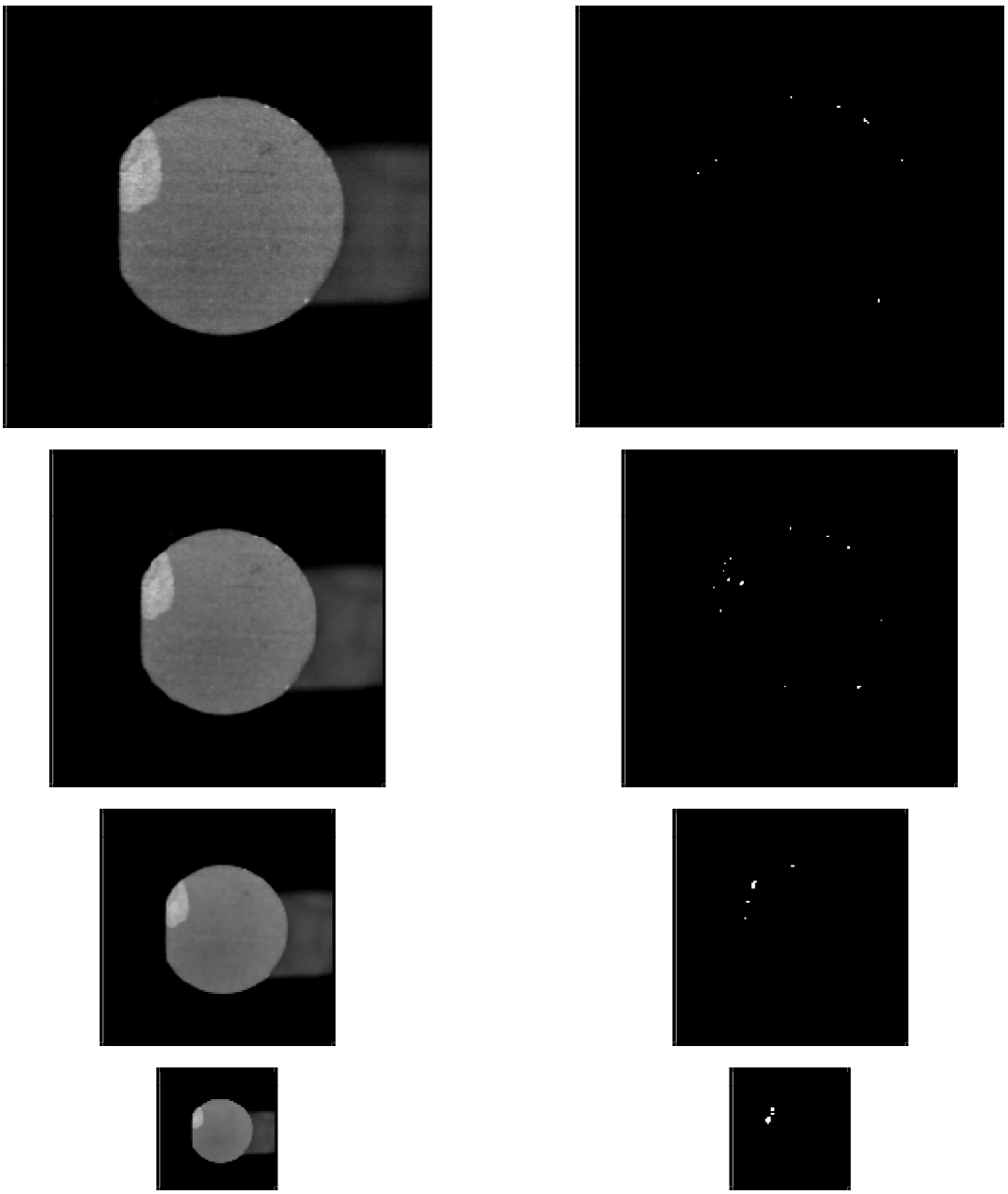

Fig. 8. The pyramid of the images of the ferrite core and the corresponding maps of defects

A typical example of the input images of the core and of the maps of defects is illustrated by successive rows in Fig. 8. The images in the left column show the view of the end part of the core having the form of the letter U and have 256 gray levels. The images at the top level are of size 512*512 pixels. In order to be able to detect defects independently of their size, one has to resort to the use of a morphological pyramid. As illustrated by the left column of Fig. 8, successive levels of the pyramid are generated by reducing the resolution of the images by two, so that the images in the second level are of size 256*256 pixels, and so on (smaller images have been enlarged in the figure for better visibility). The reduction of the size of the image usually involves some loss of information. However, it was assumed in this case that the morphological pyramid is generated in such a way that each successive image is obtained from the previous (larger) one by means of the morphological filtering in the form of closing followed by opening, with subsequent sampling of the filtered image. The purpose of the filtering is the removal of noise from the image while keeping the loss of useful information about the defects at a minimum.

One can notice that the operations of closing and opening used for pyramid generation are of the same type as the operations of closing and closing needed by the defect detector. In fact these operations are performed on the same images and in the same sequence so that they can be carried out only once. In this way a significant reduction of the processing time is achieved. Summarizing, the gray level maps are generated for all levels of the pyramid.

As was mentioned before, the defect detector generates a noisy output. Removal of the pixels with low measure of defectiveness is carried out by the software for data reduction. The crucial step in data reduction is thresholding, which converts the gray level maps of defects into binary maps, in which defects include only those pixels for which the measure of defectiveness exceeds a specified threshold. In binary maps, such as shown in the right column of Fig. 8, the pixels representing defect-free area are black (brightness 0), and the pixels belonging to defects are represented by white (brightness 255). The thresholds for binarisation greatly influence the outcome of the defect detection system, and have to be selected for all levels of the pyramid. The optimization of the thresholds is time consuming and has to be repeated whenever the lighting conditions have changed. For speeding up the process of threshold optimization a genetic algorithm was developed, which is described in the companion paper [NN97]. The data reduction software includes also a standard labeling algorithm which labels all connected components (sometimes called blobs), in a binary image, in this case – a binary map of defects. In summary, the following data are obtained from the defect detection system: coordinates of the pixel belonging to a defect, the label (ordinal number) assigned to the defect to which the given pixel belongs, and the measure of defectiveness of the pixel.

One can observe in Fig. 8 that by using the morphological pyramid one is able detect defects of various sizes. At the top level small bright defects on the border of the core are detected, whereas the huge defect in the upper left quadrant of the image remains undetected. At lower levels of the pyramid larger and larger defects are detected. At the second and third levels the largest bright defect is detected only in part; in fact there are several disconnected blobs at the site of the defect. At the fourth level the blobs cover most of the surface of the huge defect. The enclosed detection example clearly shows that the small defects are detected at a high resolution, and large defects at a low resolution. Using the same 3*3 structuring element one effectively increases the size of the structuring element in comparison with the low resolution image so that the same small structuring element is sufficient for all levels of the pyramid. Furthermore, the reduction of the size of images results in reduction of the processing time. No special attempts were made to develop software for so called fast morphological operations. Nevertheless, the overall processing time for the 4-level pyramid starting with the image of 512*512 pixels is about 1 second.

The described defect detection system indicates the defects. However, it is unable to assign pixels to predefined classes of defects. The output of the defect detection system is subsequently used by the defect classification system described in the following.

6. Feature-based classification of the detected regions

The pixels marked in the detection phase are treated as patterns for further classification. Each single pixel is a pattern. Its features are found as functions defined on its square neighbourhood, called the *simple neighbourhood*. To have direction-invariant features, besides a simple one, a *rotated neighbourhood* is used. The edges of the rotated neighbourhood are placed along the dominating direction of texture, calculated locally in the simple neighbourhood, according to the spectral method proposed in [YBF95]. The final equation for direction, derived there, is very simple:

$$\tan(2\theta - \frac{\pi}{2}) = \frac{\iint_\Omega 2\,\frac{\partial I}{\partial x}\frac{\partial I}{\partial y}\,dx\,dy}{\iint_\Omega \left[\left(\frac{\partial I}{\partial x}\right)^2 + \left(\frac{\partial I}{\partial y}\right)^2\right] dx\,dy} \qquad (2)$$

where Ω is the area of the simple neighbourhood. An example of a simple and a rotated neighbourhood is shown in Fig. 9.

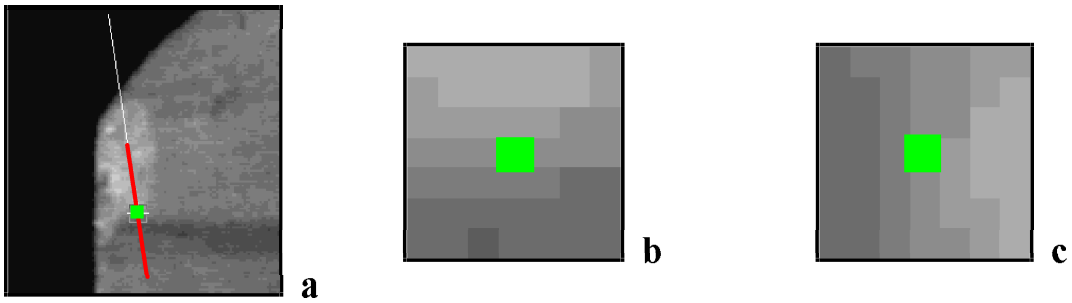

Fig. 9. a: pixel with the normal to the dominating direction of texture marked; b: simple 7*7 neighbourhood of this pixel, used for direction calculation; c: rotated 7*7 neighbourhood

Several groups of features have been tested. Those intrinsically rotation invariant were calculated from the simple neighbourhood only. The list of the considered features follows:

1. raw brightnesses in the simple neighbourhood;
2. raw brightnesses in the rotated neighbourhood;
3. statistical moments of brightnesses in the simple neighbourhood, of order 2 up to *R*;
4. same as 3, but in the rotated neighbourhood;
5. modulus of gradient in the simple neighbourhood;
6. textural features according to [Law80], described also in [Pra91];
7. same as 6, but in the rotated neighbourhood;
8. textural features based on the concurrence relations according to [WuCh92];
9. same as 8, but in the rotated neighbourhood;
10. section of brightnesses function along the line according to θ.

In the experiments, from 30 to 150 features were used at a time. Larger numbers would also be applicable in the recognition phase, but they would be too much time-consuming for the feature selection algorithms.

The feature set selected as optimum at the present stage of studies consists of all 9 features of group 7 (features 1-9) and 21 features of group 10 (features 10-30).

The group 10, proposed within the Project, needs a short explanation. The *section of brightnesses function* has been designed to reflect long–distance brightness relations, with large number of features like in groups 1 and 2 avoided. A line section centred at the pixel of interest, according to the dominating texture direction (as marked with a broader line in Fig. 9a) is drawn in the picture. It passes through other pixels which lie symmetrically around this central pixel. Let us index the central pixel with index 0, the pixels towards darker region of the image with positive indexes, and towards the opposite direction with negative indexes. Then, the subsequent features are calculated as indicated in Table 1.

feature	1	2	3	4	5	...
value	I(0)	I(1)/I(0)	I(-1)/I(0)	I(2)/I(0)	I(-2)/I(0)	...

Table 1. Calculation of features from group 10 (see text)

The selected features made it possible to get very satisfactory results of final recognition (see sections 9 and 10).

7. *K nearest neighbours* classification

The well known classification method of *k nearest neighbours* (k-NN) has been used [Bez86, Das95]. The basic version of this method is the following. Assume that a set of patterns from each class is given. The sum of these sets is called the training set. To recognise an unknown pattern it is necessary to find its k nearest neighbours in the feature space. The unknown pattern is assigned to the class to which the majority of these k neighbours belong.

The method is known for very quick training. Actually, no training is needed in a sense like for example in case of a neural network. Training a k-NN classifier is carrying out feature selection and choosing the value of k. This can be done effectively, even with simple strategies of search in the parameter space. A good criterion is minimum overall error or minimum of the maximum inter-class error. This criterion has been used in the present work. Errors can be precisely estimated on the whole available set of training patterns with the use of the *leave-one-out* method.

Here, a highly advanced version of the k-NN method has been used. It can be described by the following properties:

1. fuzzy [Joz83];
2. parallel (there is a separate classifier for each pair of classes, and the classifiers vote);
3. with full selection of features and k (separately for each classifier);
4. hierarchical (a simple 1-NN version is used where classes do not overlap in the feature space) [Joz96];
5. with reduced reference patterns set (sets of reference patterns for classes contain only those training patterns which influence the class boundaries in the feature space).

The properties 1, 2 and 3 improve the quality of classification. Property 3 gives some improvement in efficiency as a side-effect. Properties 4 and 5 have been introduced exclusively for efficiency. They make it possible to reach a desired point in the efficiency-quality trade-off. In the present work the requirement of classification quality has been promoted, and the reference patterns set has been reduced as much as possible, but without letting the recognition results change to worse for any initial training pattern. Intensive work on further speeding up the classification algorithm is currently being carried out.

8. Training patterns

For training, the *ground truth* data have been provided by *manually* marking with colours the pixels which belong to classes in the training images, made of the training batch of cores. This difficult task has been possible to fulfil only with looking at the original core. Frequently a looking glass was helpful.

The colour codes shown in Fig. 10 have been used. Please note that *artificial, boundary classes* formed with pixels lying at the boundaries between physical classes have been introduced. This has led to better accuracy, as it has become possible to perform the choice of classifier parameters for more specific class pairs.

Due to the reasons described in section 3, class 9 was merged with 6, and class 10 with 7. Class 11 was not represented in the training batch of cores. Hence, finally there were 8 classes.

In the initial experiments as much as 50,000 pixels have been used for training. Later, with the insertion of the boundary classes, less than 10,000 training pixels were used. The results presented further were obtained with the numbers of training patterns as shown in Table 2.

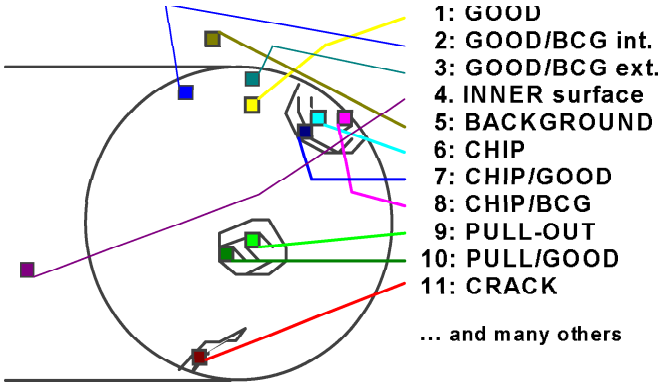

Fig. 10. Colour codes of classes and boundary classes (see text)

class #	class name	no. of pixels
1	GOOD	1382
2	GOOD/BCG int.	324
3	GOOD/BCG ext.	479
4	INNER surface	1195
5	BACKGROUND	1249
6	CHIP	188
7	CHIP/GOOD	181
8	CHIP/BCG	205
	Total	**5903**

Table 2. Numbers of training patterns (pixels) used in the presented examples

9. Results of training

From numerous data obtained from the training, such as features selected for pairs of classes, class pairs errors, sequence in which features have been selected, resulting reduction of reference sets for class pairs etc., the final inter-class errors are of main interest for the end-user.

The overall error obtained, estimated on the whole training set, has been **2.56 %**. The inter-class errors can be seen in Table 3. A maximum of 9 % between classes 8 and 6 must be taken into account by the postprocessing stage.

The frequencies of selecting the features for the 28 pairwise classifiers is shown in Table 4. It can be seen that the *section of brightnesses* features (group 10) has been well chosen.

	1	**2**	**3**	**4**	**5**	**6**	**7**	**8**
1	97					0.4		2
2		95	0.3	**4**			0.6	
3		0.6	97	0.2	0.2		2	
4		0.2		99.8				
5					99.9		0.08	
6	0.1					95		***5***
7			**4**		**3**		92	
8	**3**					***9***		88

Table 3. *A posteriori* error probabilities: that pixel classified as class "i" (row) comes in fact from the class "j" (column); in %, zero values omitted

feature	1	2	3	4	5	6	7	8	9
frequency	9	3	0	10	7	4	4	4	2

feature	10	11	12	13	14	15	16	17	18	19	20	21	22	23	24	25	26	27	28	29	30
frequency	**15**	***17***	3	6	2	3	3	5	5	5	6	4	6	5	3	4	5	6	6	5	10

Table 4. Frequencies of selecting the features for use in classifiers for pairs; above: Laws textural features (group 6); below: *section of brightness* features (group 10)

10. Examples of results

In the results below, we shall exemplify with images a number of phenomena:

1. overall quality of classification (Figs. 11-13);
2. small differences between the results obtained without and with the reduction of the reference patterns set, while the reduction gave about 14 times classification speed-up (Fig. 11);
3. generalisation power of the classifier: correct results for pixels not used for training (Figs. 12, 13);
4. invariance of results to small lighting changes (besides that light stability is guaranteed) (Fig. 12);
5. invariance of results to rotation and shift (Fig. 13).

The time of classification of 1000 pixels was about 7 s (Pentium 200 Mhz, 32-bit software – GNU C). In a typical 512*512 image, about 800 pixels are selected for classification.

In the figures, the results of postprocessing are also shown. The methodology of postprocessing will be outlined in the following section.

11. Postprocessing: convex hull and merging

The vast majority of the irregularities are *convex*. On the other hand, the detector as well as the classifier tend to make errors inside larger defects. It is a straightforward idea to span a *convex hull* over the blobs which represent irregularities (this is class number 6, see Fig. 10). The experiments indicate that indeed this improves the quality of classification results.

That some parts of a defect can be missed by the detector or the classifier implies that merging some blobs which are near to each other in the image could also improve the results. Strategies of merging are now under discussion. The evidence given by the boundary classes of the irregular class (classes 7 and 8) should be taken into account. It seems clear that those classes for which the classification errors are small (class 7, Table 3) should be used in another way that those for which these errors are large (class 8). This will be the subject of further studies.

At present, the merging is carried out as follows: class 7 is merged with class 6, and blobs formed in this way which are closer to each other by less than 6 pixels are merged. Spanning the convex hull over the resulting blobs is made afterwards. Examples of results can be seen in the Figs. 12 and 13, and in Fig. 14 below. In the latter figure an untypical, extraneously bad result of classification is presented to illustrate the potential of the postprocessing method.

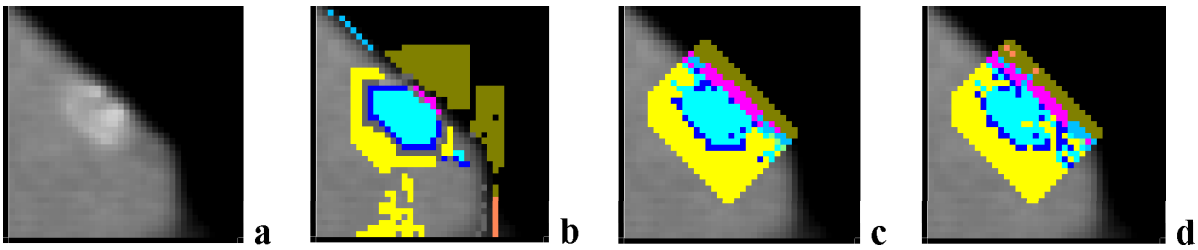

Fig. 11. Classification of trained pixels: a: original; b: training data; c: classified without reduction of ref. pat. set; d: classified with reduction; generalisation power of the classifier suffered very slightly

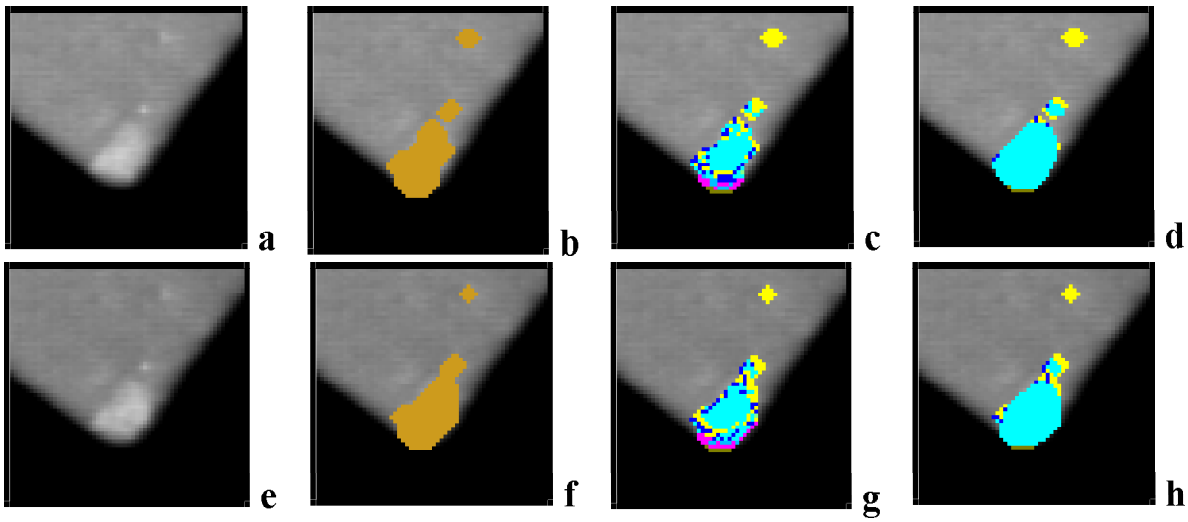

Fig. 12. Generalisation power of the classifier and invariance to small lighting changes: a-d: light I; e-h: light II; a, e: originals; b, f: detected regions (by pyramid); c, g: classified with reduction of reference set; d, h: postprocessed; results for light I and II do not differ much

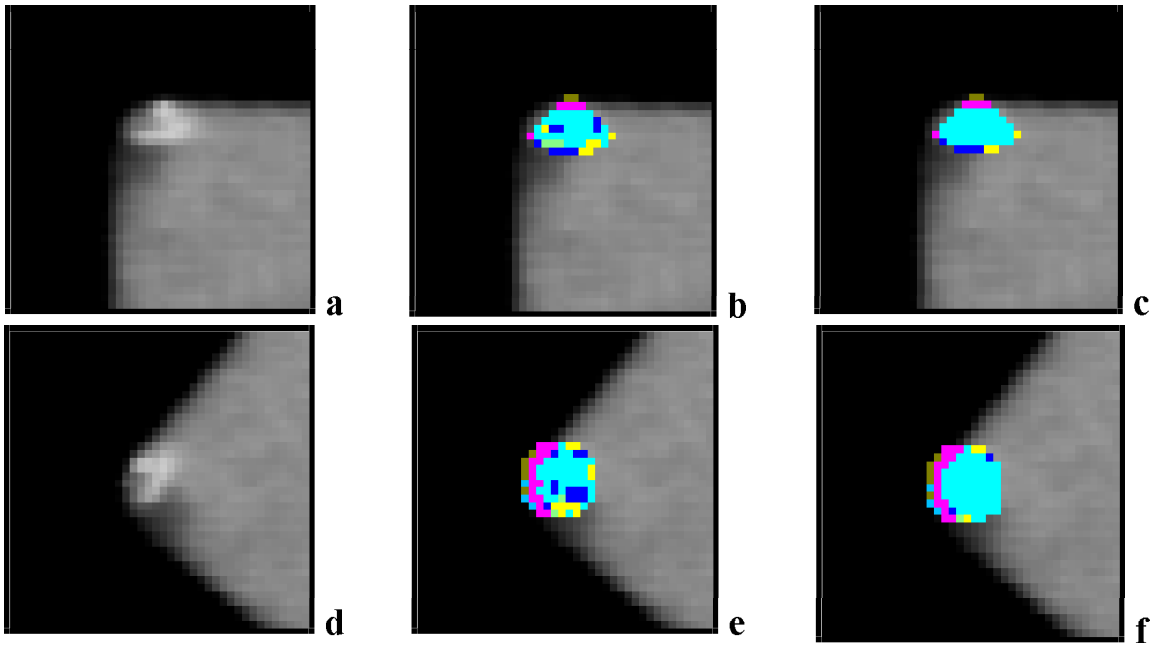

Fig. 13. Generalisation power of the classifier and invariance to rotation and shift of the tested object: a-c: position I; d-f: position II; a, d: originals; b, e: classified with reduction of reference set; c, f: postprocessed; results for position I and II do not differ much

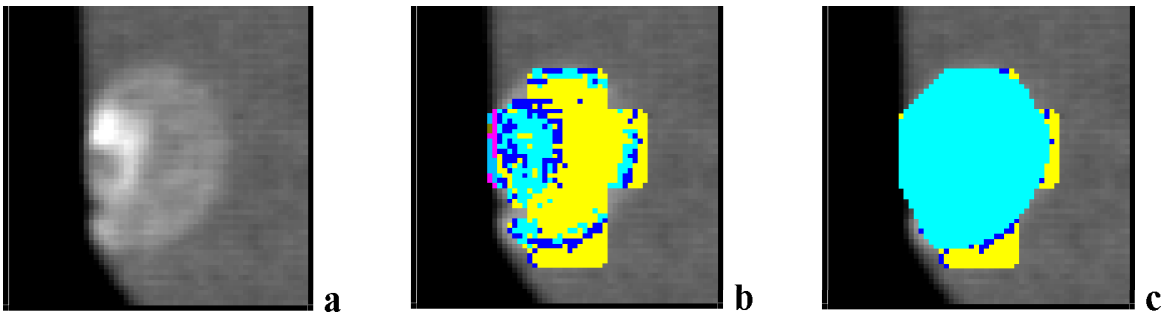

Fig. 14. a: original image a very large chip; b: classified; c: postprocessed (see text)

12. Conclusion

A hierarchical computerised optical inspection system for detection and classification of defects (called *irregularities*) on mating surfaces of ferrite cores has been designed and implemented. Special attention was paid to overcoming the difficulties related to dark colour of the tested objects and to attain invariance of the phases of inspection to such noncontrollable factors like scale of the defects and location of the object. The system has been found to work properly in a series of tests. Quantitative nature of the results make it possible to carry out various kinds of analyses of the production process.

It is planned to develop the system up to an industrial level. For this purpose, no other highly specialised hardware seem to be necessary than a mathematical morphology processor. The proposed methodology is applicable to detection of defects on flat surfaces of numerous similar (black ceramic, magnets) and dissimilar materials.

Acknowledgement

The research has been carried out within the COPERNICUS programme, under the projects: *CRAck and SHape defect detection in ferrite cores* (CRASH) no. COP - 94 00717 in 1995-96 (see the WWW site at "http://www.lii.unitn.it"), and *Standard compliant QUAlity control System for High-level ceramic material manufacturing* (SQUASH) no. ERBIC 15CT 96 0742 in 1997-98 (the WWW site of the project is reachable from the page "http://aetnet.it/Aet/aet.htm"). The projects have been realised by a multinational consortium. The presented results were obtained by the teams of the Association for Image Processing (Towarzystwo Przetwarzania Obrazów, "http://www.tpo.org.pl") and Institute of Biocybernetics and Biomedical Engineering, PAS (Instytut Biocybernetyki i Inżynierii Biomedycznej PAN). The end-user of both projects has been POLFER Magnetic Materials Co.Ltd. (Zakład Rdzeni Magnetycznych POLFER Sp. z O.O.), Warsaw.

References

[Bez86] J.C. Bezdek, S.K. Chuan, D.Leep, Generalized k-NN rules, *Fuzzy Sets and Systems*, **18**, 1986, pp. 237-256.

[Das95] B.V. Dasarathy, Nearest Neighbor (NN) norms: NN pattern classification techniques, *IEEE Computer Society Press*, 1995.

[EPS97] *Light systems for testing the surface irregularities of ferrite cores*, EPSILON® ARG Ltd, Jan 1997 (annex to FMCL97).

[FMCL97] F. Fontana, M. Mari, D. Chetverikov, M. Lugg, T. Postupolski, A. Jóźwik, M. Skłodowski, M. Nieniewski, W. Cudny, L. Chmielewski, *CRAck and SHape defect detection in ferrite cores – Final Technical Report of the project CRASH*, CRASH Consortium, Jan 97.

[Joz83] A. Jóźwik. A learning scheme for a fuzzy k-NN rule. *Pattern Recognition Letters*, **1**, 1983, pp. 287-289.

[Joz96] A. Jóźwik, L. Chmielewski, W. Cudny, M. Skłodowski, A 1-NN preclassifier for fuzzy k-NN Rule, *Proc. 13th Int. Conf. Pattern Recognition*, Wien, Austria, Aug 25-29, 1996, pp. D-234 - D-238.

[Law80] K. I. Laws, Textured image segmentation, Univ. of Southern California, Image Processing Institute, *USCIPI Report* 940, Jan 1980

[Nie97] M. Nieniewski, Morphological method of detection of defects on the surface of ferrite cores, *Proc. 10th Scandinavian Conf. Image Analysis*, Lappeenranta, Finland, June 9-11, 1997, pp. 323-330.

[NN97] T.C. Nguyen, M. Nieniewski, Using genetic algorithm for optimisation of the thresholds in the morphological pyramid for detecting defects on the surface of ferrite cores, *Proc. 3rd Symp. Image Processing Techniques*, Oct. 29-31, 1997, Serock. In this volume.

[Pra91] W. K. Pratt, *Digital Image Processing*, John Wiley, New York 1991.

[YBF95] G. Z. Yang, P. Burger, D. N. Firmin, S. R. Underwood, Structure Adaptive Anisotropic Filtering for Magnetic Resonance Image Enhancement, *Proc. 6th Int. Conf. CAIP*, Prague, Czech Republic, Sept. 6-8, 1995, 384-391. Lecture Notes on Computer Science. Springer Verlag, 1995.